

Application of Model-Based Methods to Characterize Exenatide-Loaded Double-Walled Microspheres: *In Vivo* Release, Pharmacokinetic/Pharmacodynamic Model, and *In Vitro* and *In Vivo* Correlation

XINGANG LI,¹ LIANG LI,² XIPEI WANG,¹ YUPENG REN,¹ TIANYAN ZHOU,^{1,2} WEI LU^{1,2}

¹Department of Pharmaceutics, Peking University, Beijing 100191, People's Republic of China

²State Key Laboratory of Natural and Biomimetic Drugs, Peking University, Beijing 100191, People's Republic of China

Received 20 February 2012; revised 3 May 2012; accepted 30 May 2012

Published online 29 June 2012 in Wiley Online Library (wileyonlinelibrary.com). DOI 10.1002/jps.23236

ABSTRACT: The objective of this study was to characterize exenatide double-walled microspheres (DWMS) using model-based methods. Exenatide DWMS were prepared using oil-in-oil-in-water method, and physicochemical characterization and *in vitro* release and degradation of DWMS were evaluated. The pharmacokinetics (PK) and pharmacodynamics (PD) were investigated after subcutaneous injection to diabetic rats. Transit compartment model was used to describe the *in vivo* release of exenatide from DWMS successfully. On the basis of the insulinotropic effects of exenatide and hypoglycemic effects of insulin, PK/PD model was developed and nicely described the concentration–effect relationship of exenatide. Moreover, on the basis of the transit compartment model, a simulation method was applied to predict *in vivo* release, and *in vitro* and *in vivo* correlation was established. In conclusion, DWMS was a promising vehicle for delivery of exenatide, and the proposed PK/PD model allowed a better understanding of the pharmacological properties of exenatide DWMS. Transit compartment model-based modeling and simulation methods provided more options for the description and prediction of the *in vivo* exenatide release from DWMS. © 2012 Wiley Periodicals, Inc. and the American Pharmacists Association *J Pharm Sci* 101:3946–3961, 2012

Keywords: exenatide; double-walled microspheres; controlled release; transit compartment model; dose-response; pharmacokinetic/pharmacodynamic model; simulation; *in vitro* and *in vivo* correlation

INTRODUCTION

Exenatide, glucagon-like-peptide-1 (GLP-1) analogue and the first clinically available incretin mimetic, possesses many glucoregulatory functions and ameliorate endocrine pancreatic functions by stimulating glucose-dependent insulin secretion, suppressing glucagon secretion, reducing gastric mobility and food intake, and stimulating pancreatic β -cell proliferation and/or neogenesis.^{1–3} Moreover, exenatide was more potent than GLP-1 and demonstrated a greater maximal effect than GLP-1 *in vivo*.^{2,4} It was autho-

rized for marketing in the European Union in November 2006 and was approved by US Food and Drug Administration (FDA) in April 2005.⁵ Furthermore, FDA approved BYDUREON™ (exenatide extended-release microspheres)—the first once-weekly treatment for type 2 diabetes in January 2012. However, BYDUREON™ is prepared using the complicated method of water-in-oil-in-oil coacervation, and improper release of exenatide from BYDUREON™ leads to the poor pharmacokinetics (PK) and efficacy.⁶ Sustained-release microspheres of exenatide based on different preparation methods and biodegradable materials have also been studied.^{7–9}

Comparing with single-layer microspheres, double or multi-walled microspheres are more advantageous. Since a single-step technology for double-walled microspheres (DWMS) preparation was first reported,¹⁰ DWMS found a preferable sustained-release carrier,

Correspondence to: Tianyan Zhou (Telephone: +86-10-82805763; Fax: +86-10-82805763; E-mail: tianyanzhou@bjmu.edu.cn); Wei Lu (Telephone: +86-10-82801717; Fax: +86-10-82801717; E-mail: luwei_pk@bjmu.edu.cn)

Journal of Pharmaceutical Sciences, Vol. 101, 3946–3961 (2012)
© 2012 Wiley Periodicals, Inc. and the American Pharmacists Association

and more and more investigations focused on it.^{11–13} The DWMS with distinct core/shell structures achieved distinct degradation behavior.^{14–16} On the one hand, the rapid degradation and accelerated erosion of the polymer core result in the production of a hollow structure in the center of DWMS. On the other hand, the polymer shell remains relatively intact due to its slow degradation characteristics. The distinct structure and degradation behavior of DWMS make it possible to be used as an improved drug delivery system that can increase EE, alleviate burst effect, and make drug release constantly and persistently.

The absorption of drugs from the gastrointestinal tract is very complex and not well characterized using a first-order absorption model.¹⁷ Many researchers use transit compartment model to characterize the transit process of oral dosage forms through the whole gastrointestinal tract.^{18,19} The process of drug passing through the whole gastrointestinal tract was viewed as flow through a series of segments and this model is close to the real process. In addition, Sun et al.²⁰ reported that the delayed drug effects due to the signal transduction processes can also be well described by transit compartment model, and the later reports supported this approach.^{21,22} Transit compartment model is a good tool to describe the process of drug delivery and signal transduction.

Pharmacokinetic and pharmacodynamic (PD) models are valuable tools to describe and predict the *in vivo* performance of a certain drug.²³ PK/PD modeling can be used to quantitatively describe the relationship between drug concentration and biological response. It is good for rational design of dosing regimen and clinical application, with the benefit of modeling and simulation. Extensive PK/PD modeling was applied to characterize the glucose level and insulin system in various circumstances.^{24,25} PK/PD model can also be used to evaluate the dosage form,²⁶ optimize molecular weights of prodrug,²⁷ and select a promising prodrug.²⁸ Model-based method is becoming more and more important and practical in drug research and development.

Aim of *in vitro* and *in vivo* correlation (IVIVC) was to use the *in vitro* release data as a surrogate for bioequivalence studies. The *in vivo* release of drug could be calculated from PK using Wagner–Nelson, Loo–Riegelmanor, and deconvolution methods.^{29,30} Direct measurement³¹ and differential equation-based IVIVC method³² were also proposed. However, to the best of our knowledge, there is no report using an approach based on transit compartment model to evaluate the *in vivo* release profile and IVIVC of microspheres.

The aims of this study were to structure near-constant release DWMS and evaluate its characteristics by model-based methods. Exenatide DWMS were prepared using oil-in-oil-in-water ($O_1/O_2/W$) method.

Transit compartment model was proposed to describe *in vivo* release of exenatide from DWMS after subcutaneous (s.c.) administration to diabetic rats. On the basis of the action mechanisms of exenatide and insulin, the PK/PD model was developed to describe the complete time course of the blood glucose-lowering effect (GLU) under different doses. Finally, using transit compartment model-based simulation method to establish IVIVC was addressed.

MATERIALS AND METHODS

Materials

Exenatide (purity >99%) was purchased from Shanghai Taishi Biotechnology Company, Ltd. (Shanghai, People's Republic of China). Poly(D, L-lactide-co-glycolide) (PLGA, DG-50DLGH025, lactide–glycolide molar ratio is 50/50 and inherent viscosity is 0.15–0.25 dL/g) and poly(L-lactide) (PLLA, DG-L150, inherent viscosity is 1.1–1.5 dL/g) were purchased from Daigang Biotechnology Company, Ltd. (Jinan, People's Republic of China). Polyvinyl alcohol-124 (PVA 124, 98.8% hydrolyzed) was produced by East Ring Union Chemical Plant (Beijing, People's republic of China). Streptozotocin (STZ, Sigma No. S0130) was purchased from Sigma–Aldrich (St. Louis, Missouri). Fluorescein isothiocyanate (FITC)–insulin was purchased from Sigma (St. Louis, Missouri). Sodium carboxymethyl cellulose (CMC-Na), Tween 20, sodium chloride (NaCl), phosphate-buffered saline (PBS), and other chemicals were of analytical grade.

Preparation of DWMS

An $O_1/O_2/W$ emulsion solvent evaporation method was used to fabricate DWMS. Exenatide (4 mg) and 70 mg PLGA dissolved in 1.4 mL mixed solvent [dichloromethane (DCM)–methanol (MeOH) = 2:1 (v/v)] was the O_1 phase, and 30 mg PLLA dissolved in 0.6 mL mixed solvent was the O_2 phase. Mixed the O_1 and O_2 phase and vortexed for 15 s. The mixed O_1/O_2 was subsequently injected into a 50 mL aqueous solution of 1% (w/v) PVA and 0.9% (w/v) NaCl. The mixture was continuously stirred at 600 rpm in ice bath for 4 h and then at room temperature for another 4 h, during which the solvent was completely evaporated. The resultant DWMS were collected by centrifugation (3000g for 2 min), washed three times with water for injection, and freeze dried. The vacant DWMS were prepared using the same method without exenatide. To satisfy the need of subsequent experiments in diabetic rats to investigate the PK and PD properties of DWMS, exenatide-loaded DWMS and vacant DWMS were prepared for many times in different batches. The relative standard deviation values of between-batch for both exenatide loading and encapsulation efficiency (EE) were less than 3%. So we thought that

the method for preparation of DWMS was stable and we accordingly combined DWMS prepared in different batches and used them in animal treatment if needed.

Physicochemical Characterization of DWMS

Particle Size and EE

The mean particle size was determined for an aqueous dispersion of DWMS using a laser particle size analyzer (BT-9300H, BETTER, Dandong, People's Republic of China). For determining drug loading, 10 mg lyophilized DWMS were dissolved in 1 mL dimethyl sulfoxide, then 10 mL of 0.05 M NaOH solution containing 0.5% (w/v) sodium dodecyl sulfate was added to it and incubated for 1 h at room temperature.³³ The exenatide concentration of incubation solution was measured by Micro bicinchoninic acid (BCATM) protein assay kit (Pierce, Illinois).⁷ The exenatide loading percentage (w/w, exenatide content per dry DWMS) was calculated. The EE was calculated by comparing the actual exenatide loading with the theoretical exenatide loading.

Surface and Cross-Sectional Morphology

The surface morphology and internal structure of DWMS were examined by scanning electron microscope (SEM; JEOL JSM-5600LV, Tokyo, Japan). After the DWMS had been dispersed in embedding agent, poured onto metal stub, and frozen at -20°C for 0.5 h, they were then cut into around 50 μm thickness slices. Deionized water was added to dissolve the embedding agent of these slices and the dissected DWMS were collected by centrifugation at 2500g for 5 min. The collected DWMS were washed three times in room temperature and were dried under vacuum. The DWMS and the dissected DWMS were evenly sprinkled onto a carbon adhesive disk mounted onto an aluminum stub. Samples were coated with a thin layer of gold and viewed using a JEOL JSM-5600LV operating at 10 kV, 20°C , and 10^{-5} Torr.

Exenatide Distribution in DWMS

Using FITC-insulin as the indicator, the drug distribution in DWMS was identified by confocal laser scanning microscopy (CLSM). The FITC-insulin-loaded DWMS were prepared in the same manner as described in *Preparation of DWMS*, except that exenatide was replaced by FITC-insulin. The FITC-insulin-loaded DWMS were cut as described in *Surface and Cross-sectional Morphology*. Then they were mounted on a slide with coverslip and visualized using a confocal imaging system (Leica TCS SP2, Heidelberg, Germany) and krypton/argon laser (excitation wavelength at 488 nm and emission wavelength at 505 nm).

Exenatide Secondary Structure Study

Exenatide conformation and change thereto was characterized using circular dichroism (CD). CD spectra were recorded at room temperature using spectropolarimeter (J-810 spectropolarimeter, Jasco, Japan) for each of the exenatide samples in the far ultraviolet region (185–250 nm) in a 0.1 cm path length cell using a step size of 1 nm, and an average of three scans was obtained. Exenatide aqueous solution (100 $\mu\text{g}/\text{mL}$) was used as control. Exenatide samples were extracted from DWMS as follows: 11 mg DWMS dissolved in 0.5 mL DCM. Then 2 mL deionized water was added into the solution, vortexed for 2 min, and centrifuged at 4250g for 10 min. Supernatant was decanted into fresh tube and stored at 4°C until analysis.

In Vitro Release and Degradation of DWMS

DWMS (30 mg) were suspended in 1.0 mL PBS (pH 7.4) containing 0.02% (w/v) Tween 20. The suspension was incubated at 37°C under continuous agitation (100 rpm) for 70 days. At predetermined intervals, samples were centrifuged, 0.8 mL supernatant was withdrawn, and equal volume of fresh release medium was added. The concentration of exenatide in the supernatant was determined by Micro BCATM protein assay kit. The cumulative release amount was calculated by:

$$\%M_r = \frac{0.8 \times \sum_1^{i-1} C_{i-1} + C_i}{M_{\text{ex}}} \times 100 \quad (1)$$

M_r and M_{ex} represent the amount of cumulative release and total amount of exenatide in DWMS, respectively. C_i and C_{i-1} are concentrations of supernatant at the i th and $i-1$ th sampling, respectively.

Four aliquots of 20 mg DWMS were dispersed in 1.0 mL PBS (pH 7.4) containing 0.02% (w/v) Tween 20. The suspensions were dispersed in tubes and stirred at 100 rpm in an air chamber thermostated at 37°C . At the specific time point (4, 20, 40, and 70 days), one aliquot of DWMS was collected by centrifugation (2500g for 5 min) and cut as described in *Surface and Cross-Sectional Morphology*. The internal structures of DWMS were examined by SEM.

Animals and Treatment

Induction of Experimental Diabetes in Rats

All animal experiments were carried out following the Guide for Care and Use of Laboratory Animals as adopted and promulgated by the Animal Ethics Committee of Peking University Health Science Center (Beijing, People's Republic of China). Male Sprague-Dawley rats weighting 190–210 g were obtained from the Experimental Animal Center at the Peking University Health Science Center. The diabetic rats were

induced using high-fat diet/STZ treatment method.³⁴ Briefly, all rats were housed under standard conditions with a 12 h dark/light cycle and an ambient temperature of 22°C–25°C, and free access to a high-fat diet (20% sucrose, 10% lard, 2% cholesterol, 1% cholate, and 67% normal chow diet; Keaoxili Company, Ltd., Beijing, People’s Republic of China) and water was allowed throughout the study period. After 5 weeks, rats were anesthetized with diethyl ether after an overnight fast (free access to water) and injected intraperitoneally with 45 mg/kg STZ in 1% (w/v) citrate buffer (pH 4.3). Rats had free access to food and water after the STZ injection. After 3 weeks, rats were fasted for overnight (12 h) and blood glucose concentrations were determined by ACCU-CHEK® Advantage II (Roche Diagnostics, Germany). Blood glucose levels of at least 16.7 mmol/L were accepted as the basal level for diabetes.

Treatment

Twenty diabetic rats were randomly divided into four groups with three treatment groups and one control group. The DWMS were suspended in an aqueous vehicle (0.87% NaCl, 1.0% CMC-Na, and 0.1% Tween 20) within 2 min by vortex. The same volume of 2.0 mL aqueous suspension of DWMS with different final exenatide concentration of 0.625, 1.25, and 2.5 mg/mL was administrated by s.c. injection to three separate treatment groups, leading to the exenatide dose in each group, which was 1.25, 2.5, and 5 mg/rat, respectively. The corresponding group of control rats received only 2.0 mL suspension of vacant DWMS per rat. About 0.25 mL blood samples were collected from the orbit vein into tubes at 0 (prior to dosing), 1, 2, 4, and 10 h and 1, 3, 5, 10, 15, 20, 25, 30, 35, 40, 45, and 50 days after administration, and the blood glucose was determined using ACCU-CHEK® Advantage II simultaneously. Serum was separated by centrifugation at 8500g for 5 min and stored at –20°C until analysis.

Serum concentrations of exenatide and insulin were measured by the Exendin-4 EIA kit (EK-070-94; Phoenix Pharmaceuticals, California) and Rat Insulin ELISA kit (Groundwork Biotechnology Diagnosticate Ltd., California), respectively.

PK/PD Modeling of DWMS

PK Model

In the present study, we mainly investigate the kinetic parameters being associated with exenatide release from DWMS, which can be viewed as the process of drug flow through a series of segments before they reach absorption compartment. Each segment can be described as a single compartment with linear transfer kinetics. Therefore, release of exenatide from DWMS *in vivo* was characterized by transit

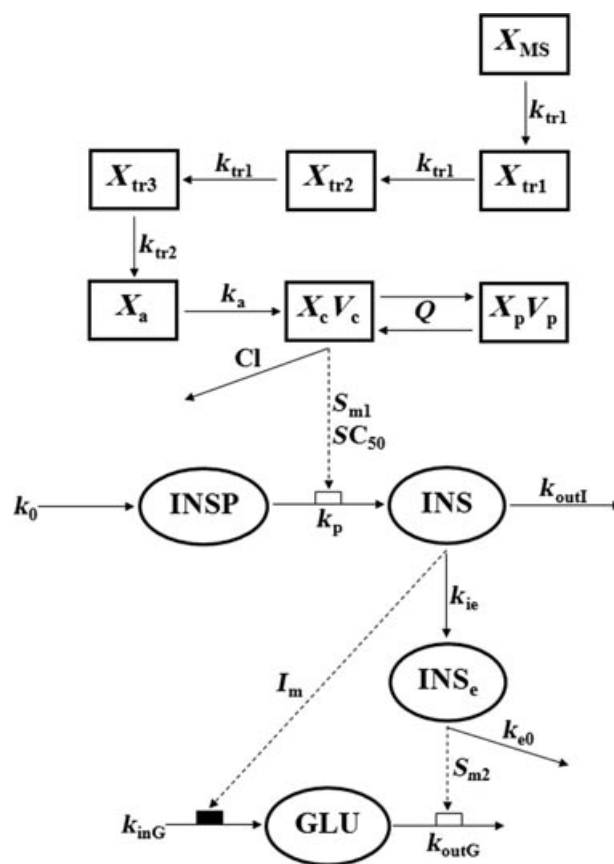


Figure 1. Schematic diagram of the proposed pharmacokinetic/pharmacodynamic model for exenatide-loaded DWMS, where X_{MS} , X_{tr1} , X_{tr2} , X_{tr3} , X_a , X_c , X_p , INSP, INS, INS_e , and GLU designate the microsphere, the first transit, the second transit, the third transit, absorption, central, peripheral, insulin precursor, insulin, effect, and blood glucose compartments, respectively. Solid lines with arrows represent the transit, absorption, elimination, or distribution of the pharmacokinetic indices, or indicate the conversions of the responses. Dashed lines with arrows and white boxes mean the stimulatory effect being exerted by the connected factors. Dashed lines with arrows and black boxes mean the inhibitory effect being exerted by the connected factors. This model accounts for the *in vivo* release of exenatide from DWMS, insulinotropic effect of exenatide, and hyperglycemic effects of insulin. The model is described by Eqs. 2–20. Definitions of parameters are provided in Tables 1 and 2.

compartment model (Fig. 1). Microsphere compartment (X_{MS}) represent the PLGA core, and the first (X_{tr1}), second (X_{tr2}), and third transit compartment (X_{tr3}) represented the three abstract compartments through which the exenatide released from PLGA core and PLLA shell to the surface of DWMS. A small quantity of exenatide was localized in the PLLA shell (Fig. 2d). Therefore, each transit compartment (X_{tr1} , X_{tr2} , and X_{tr3}) had a certain amount of exenatide with the fraction of F_{ra1} , F_{ra2} , and F_{ra3} , respectively. Owing to burst release, fraction of exenatide was directly

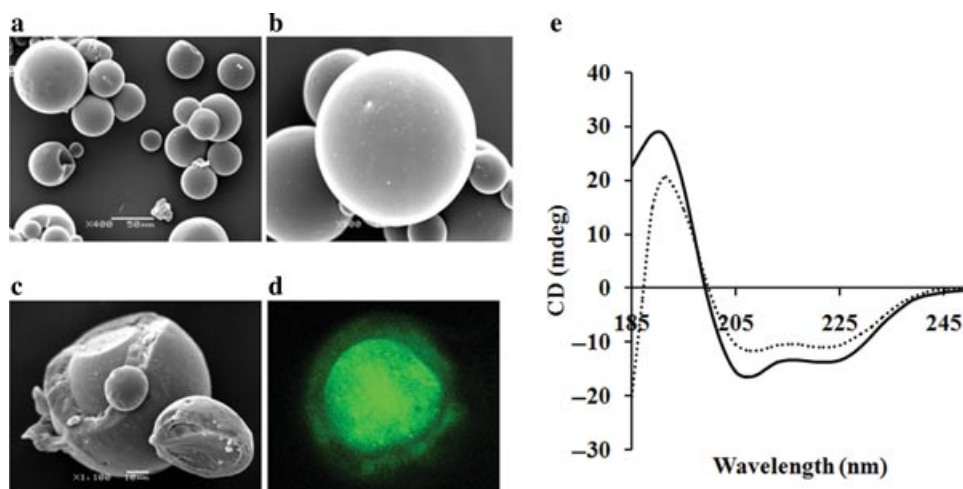


Figure 2. SEM photographs of surface morphology (a for magnification of 400, and b for magnification of 900). Cross-sectional view of DWMS fabricated with PLLA and PLGA in the mass ratio of 3:7. (c) Confocal laser scanning micrographs of the distribution of FITC-insulin in DWMS. (d) CD spectra of exenatide control (solid line) and exenatide extracted from DWMS (dotted line) (e).

released into the absorption compartment from DWMS without the transit process. Therefore, there was also a certain amount ($F_{ra4} \times D$ in Eq. 6) of exenatide in absorption compartment in the initial state. Once the exenatide released from the DWMS to circulation, the distribution and elimination of exenatide was independent of dosage form. A two-compartment PK model was used to describe the distribution and elimination of exenatide. We have obtained relevant parameters (k_a , Cl , V_c , Q , V_p) from our previous PK study.³⁵ In that study, exenatide solution was s.c. injected to STZ-treated diabetic rats, and the data from all individuals at different dose levels were fitted simultaneously. Finally, a two-compartment model with first-order absorption nicely characterized the PK behavior of exenatide. PK data of that study were rich, and the parameters were reliable. Therefore, we fixed the two-compartment model parameters as previous estimated values. In this way, we could avoid biases in the PK data, which could interfere with the estimation of the parameters of transit compartment model. The following differential equations described the above model:

$$\begin{aligned} \frac{dX_{MS}}{dt} &= -k_{tr1} \times X_{MS} [X_{MS0} \\ &= (1 - F_{ra1} - F_{ra2} - F_{ra3} - F_{ra4}) \times D] \quad (2) \end{aligned}$$

$$\frac{dX_{tr1}}{dt} = k_{tr1} \times (X_{MS} - X_{tr1}) [X_{tr10} = F_{ra1} \times D] \quad (3)$$

$$\frac{dX_{tr2}}{dt} = k_{tr1} \times (X_{tr1} - X_{tr2}) [X_{tr20} = F_{ra2} \times D] \quad (4)$$

$$\begin{aligned} \frac{dX_{tr3}}{dt} &= k_{tr1} \times X_{tr2} - k_{tr2} \times X_{tr3} [X_{tr30} = F_{ra3} \times D] \\ & \quad (5) \end{aligned}$$

$$\frac{dX_a}{dt} = k_{tr2} \times X_{tr3} - k_a \times X_a [X_{a0} = F_{ra4} \times D] \quad (6)$$

$$\frac{dX_c}{dt} = k_a \times X_a - Cl \times C_c - Q \times (C_c - C_p) \quad (7)$$

$$\frac{dX_p}{dt} = Q \times (C_c - C_p) \quad (8)$$

$$C_c = \frac{X_c}{V_c} \quad (9)$$

$$C_p = \frac{X_p}{V_p} \quad (10)$$

X_{MS0} , X_{tr10} , X_{tr20} , X_{tr30} , and X_{a0} represent initial amounts of exenatide in the microsphere, the first transit, the second transit, the third transit, and absorption compartment, respectively. D is the administration dosage, and F_{ra1} , F_{ra2} , F_{ra3} , and F_{ra4} are the scaling factors. Two transit rate constants k_{tr1} and k_{tr2} are employed here to characterize the drug release from different compartments. The exenatide in central compartment (X_c) can distribute to and from peripheral compartment (X_p) by intercompartment clearance (Q), and be directly eliminated (Cl). The fixed PK parameters (k_a , Cl , V_c , Q , V_p) are listed in Table 1.

PD Model

The modeling for drug effects was based on the fact that the insulin and blood glucose were produced with a zero-order input rate and dissipated with a first-order output rate. The PD model proposed for insulinotropic effect of exenatide is shown in Figure 1. The dynamics of insulin was characterized by an indirect response model with a precursor pool: k_0 is the zero-order precursor input rate constant, and k_p

Table 1. Parameter Estimates Obtained from the Time Profiles of Exenatide DWMS after s.c. Injection to Diabetic Rats with the Two-Compartment Pharmacokinetic Model

Parameter	Definition	Estimate (RSE%)	CV%
F_{ra1}	Fraction of exenatide in the first transit compartment ^a	0.113 (20.4)	–
F_{ra2}	Fraction of exenatide in the second transit compartment ^a	0.0301 (31.1)	130
F_{ra3}	Fraction of exenatide in the third transit compartment ^a	0.00554 (28.6)	28.8
F_{ra4}	Fraction of exenatide in absorption compartment	0.00326 (22.4)	–
k_{tr1} (h ⁻¹)	Transit rate constant 1	0.00398 (26.4)	4.0
k_{tr2} (h ⁻¹)	Transit rate constant 2	0.113 (16.4)	18.9
k_a (h ⁻¹)	Absorption rate constant	4.45 ^b	–
Cl (L/h)	Central clearance	0.198 ^b	–
V_c (L)	Central volume of distribution	0.397 ^b	–
Q (L/h)	Intercompartment clearance	0.086 ^b	–
V_p (L)	Peripheral volume of distribution	1.180 ^b	–
Residual error			
σ_1 (Proportional)	CV%	23.7	–
σ_2 (Additive)	SD ($\mu\text{g/L}$)	–	–

^aThe first, second, and third transit compartments represent the three abstract compartments through which the drug release from PLGA core and PLLA shell to the surface of DWMS.

^bParameters fixed as previous estimated values.

–Refers to the values which were fixed as 0.

and k_{outI} are the first-order precursor pool and insulin output rate constants, respectively, with the relationship

$$k_0 = k_p \times INSP_0 = k_{outI} \times INS_0 \quad (11)$$

where $INSP_0$ and INS_0 are the initial values of precursor pool and insulin compartment.

On the basis of the proposed model, the insulin change is described by:

$$\frac{dINSP}{dt} = k_0 - k_p \times \left(1 + \frac{S_{m1} \times C_c}{SC_{50} + C_c}\right) \times INSP \quad (12)$$

$$\frac{dINS}{dt} = k_p \times \left(1 + \frac{S_{m1} \times C_c}{SC_{50} + C_c}\right) \times INSP - k_{outI} \times INS \quad (13)$$

$$INS_0 = \frac{k_0}{k_{outI}} \quad (14)$$

where S_{m1} and SC_{50} are drug-specific parameters representing the maximum stimulation of the response and the exenatide concentration required for half-maximum stimulation.

A combined effect compartment/indirect response model was used to describe the relationship of insulin concentration and glucose level. Sites of action for insulin are mainly located in liver, muscle, and adipose. Liver has a robust blood supply; therefore, it is assumed that serum insulin acts directly on its corresponding receptors located in liver. However, the lack of the same robust blood supply in muscle and adipose tissue results in a distributional delay for insulin in reaching its site of action. So, an effect compartment was employed in the PD model to imitate muscle and adipose tissue, as depicted in Figure 1. Briefly, the ef-

fect compartment is distributed from the insulin compartment by first-order rate process k_{ie} , and the elimination of insulin is also characterized by a first-order rate constant k_{e0} . The insulin level in effect compartment (INS_e) is described as follows:

$$\frac{dINS_e}{dt} = k_{e0} \times (INS - INS_e) \quad (15)$$

Before administration, there was no change in INS_e ,

$$INS_{e0} = INS_0 \quad (16)$$

where INS_{e0} is the insulin basal value in effect compartment, and is equal to the base value of insulin (INS_0) in insulin compartment.

Owing to disease progression, the blood glucose increased as the time went on, both in treatment and control groups. Therefore, the GLU was defined as follows:

$$GLU = \frac{GLU_{it}^T / GLU_{i0}^T}{GLU_t^C / GLU_0^C} \quad (17)$$

GLU_0^C and GLU_t^C represent the mean blood glucose levels at time 0 and t in the control group, whereas GLU_{i0}^T and GLU_{it}^T represent the blood glucose level of i th rat at time 0 and time t in the treatment group, respectively. On the basis of normalization, the effect of disease progression on glucose level was minimized.

As we know, insulin exhibits glucoregulatory functions through increasing cellular intake of glucose in muscle and adipose tissue, and decreasing gluconeogenesis and glycogenolysis. The change of GLU is

described by the equation as follows:

$$\frac{dGLU}{dt} = k_{inG} \times [1 - I_m \times (INS - INS_0)] - k_{outG} \times [1 + S_{m2} \times (INS_e - INS_{e0})] \times GLU \quad (18)$$

where S_{m2} and I_m imitate the increasing cellular intake (it takes place in effect compartment: muscle and adipose tissue) and decreasing gluconeogenesis and glycogenolysis, respectively. The GLU starts from the basal value GLU_0 (before administration), then changes with time, following drug administration, and eventually returns to GLU_0 ($GLU_0 = 1$). Thus,

$$GLU_0 = \frac{k_{inG}}{k_{outG}} \quad (19)$$

$$k_{inG} = k_{outG} \quad (20)$$

It is assumed that change in blood glucose level is controlled by insulin level, so those parameters that describe the effect of insulin on glucose, such as k_{e0} , I_m , S_{m2} , and k_{inG} , will keep unchanged with the route of administration or dosage form of a certain drug. In this study, k_{e0} , I_m , S_{m2} , and k_{inG} were fixed as the estimated values of 0.342 h^{-1} , 0.0381 L/mU , 0.0531 L/mU , and 15.2 h^{-1} , respectively (Table 2), detected from the previous PD study in diabetic rats after s.c. administration of exenatide aqueous solution.³⁵ Other PD parameters were estimated from the model established with data collected in the present experiment.

PK/PD Analysis

A three-step approach was applied to the establishment of the PK/PD model. First, the PK parameters (k_{tr1} , k_{tr2} , F_{ra1} , F_{ra2} , F_{ra3} , F_{ra4}) were estimated except the fixed PK parameters (k_a , Cl , V_c , Q , V_p). Second, all the PK parameters were fixed, and the predicted

exenatide concentration–time profiles were used as input function for the PK/PD model. The parameters of insulinotropic effects of exenatide (S_{m1} , SC_{50} , k_0 , k_p , k_{outI}) were obtained. Lastly, the PK and insulinotropic effects parameters were fixed to these values and the GLUs-related parameters estimates were obtained. In this way, we could avoid biases in the PK data, which could interfere with the estimation of the PD parameters and *vice versa*.

A nonlinear mixed effects model analysis was performed, in which all data from different dose groups were modeled simultaneously. All of the analyses were performed using a first-order conditional estimate with INTERACTION method in NONMEM version 72 (Icon Development Solutions, Maryland). The typical values in the population were described, as well as the random effects, including the variability between subjects (parameters are log-normally distributed), the variability between occasions, and the residual variability (combination of proportional and additive error).

The ability of the PK/PD model to describe the observed data was evaluated by a visual predictive check (VPC) based on 2000 data sets that were simulated with the obtained final parameter estimates, and the median and 5th and 95th percentiles were calculated. The adequacy of the model was evaluated by comparing the distribution of observed values with that of simulated values.

In Vitro and In Vivo Correlation

The relationship between percent *in vitro* release in PBS and the percentage of absorption *in vivo* (F_a) was examined. The F_a was determined using the deconvolution and model-based simulation method, respectively. For deconvolution, the software package, WinNonlin® IVIVC Toolkit™, Version 5.2, (Pharsight Corporation, St. Louis, Missouri) was used for performing the procedure. A unit impulse response (UIR)

Table 2. Parameter Estimates Obtained from the Insulin Profiles after Single s.c. Injection of Exenatide DWMS to Diabetic Rats with PK/PD Model

Parameter	Definition	Estimate (RSE%)	CV%
S_{m1}	Maximum insulin tropic response factor	0.856 (22.2)	16.4
SC_{50} ($\mu\text{g/L}$)	Concentration for 50% of insulin tropic effect	4.04 (28.9)	29.2
k_0 (mU/L/h)	Zero-order precursor input rate constant	321 (21.4)	8.1
k_p (h^{-1})	Insulin precursor release rate constant	0.00057 (20.1)	8.6
k_{outI} (h^{-1})	Insulin output rate constant	31.9 (25.3)	–
k_{outG} (h^{-1}) ^a	Glucose output rate constant	15.2 ^b	–
S_{m2} (L/mU)	Stimulation factor of insulin on glucose disposal	0.0513 ^b	–
I_m (L/mU)	Inhibition factor of insulin on glucose production	0.0381 ^b	–
k_{e0} (h^{-1})	First-order elimination rate constant from the effect compartment	0.342 ^b	–
Residual error			
σ_1 (Proportional)	CV%	12.3	–
σ_2 (Additive)	SD (mU/L)	–	–

^a k_{outG} is equal to k_{inG} .

^bParameters fixed as previous estimated values.

–Refers to the values which were fixed as 0.

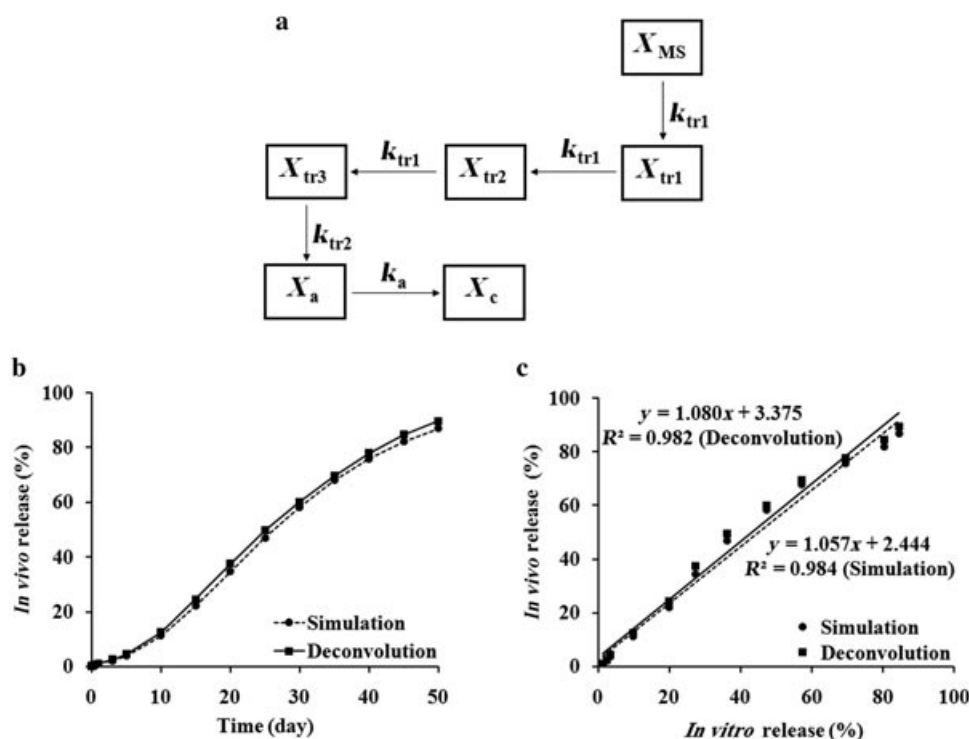


Figure 3. The proposed *in vivo* release model with three transit compartments. (a) Exenatide *in vivo* release percentage obtained from deconvolution method (solid line) and transit compartment model-based simulation method (dotted line). (b) IVIVC model linear regression plots of cumulative absorption versus percent release *in vitro* (solid line for deconvolution method and dotted line for simulation method) (c).

was assessed using the exenatide injection as a reference. The deconvolution of the mean *in vivo* concentration–time data of three doses was performed using the UIR to estimate F_a , respectively, and the mean F_a was used to establish the IVIVC with mean *in vitro* release. For the model-based simulation method, procedures were performed using NONMEM program as follows: First, PK parameters k_{tr1} , k_{tr2} , F_{ra1} , F_{ra2} , F_{ra3} , F_{ra4} , and k_a were fixed as the estimated values. The other parameters and peripheral compartment were removed from the PK model to form a new pseudo-PK model with no drug distribution and elimination, meeting the requirement of drug accumulation only in central compartment (Fig. 3a). Then, the amount of drug flowed into the central compartment were simulated at three different doses from the pseudo-PK model. The simulated amount of drug in central compartment could indicate the amount of drug absorbed in rats and the F_a could be calculated. Linear regression analysis was applied to the IVIVC plots in both deconvolution and model-based simulation method. The values of correlation coefficient (R^2), slope, and intercept were calculated, respectively.

RESULTS

Physicochemical Characterization of DWMS

The mean particle size of the exenatide DWMS was about 65.1 μm . The exenatide content in DWMS was

approximately 3.5% (w/w), and the EE was $90 \pm 2.5\%$ ($n = 3$). The SEM images showed that DWMS were orbicular and with a porous surface (Figs. 2a and 2b). The distinct double layer can be seen in the SEM photographs (Fig. 2c). The PLGA was coated with PLLA, resulting in a core and shell morphology. CLSM of DWMS encapsulating FITC–insulin showed that most of the protein was localized in the PLGA core (Fig. 2d) and low burst release could be expected. The CD spectra of exenatide control and exenatide extracted from the DWMS were shown in Figure 2e. Both of them have double peaks with minimum absorption at 222 and 208 nm, which are the typical characteristics of α -helices structure of exenatide, indicating that exenatide in DWMS maintains the secondary structure of the native exenatide. Therefore, preparation process does not alter the conformation of exenatide.

In Vitro Release and Degradation of DWMS

The *in vitro* cumulative release of exenatide from DWMS was shown in Figure 4a. Exenatide on surface or near surface of the DWMS leads to burst release. The release profiles showed approximately 1% initial burst, followed by a lag phase of about 8 days. In initial period of the *in vitro* release, as the polymer degraded slowly, the exenatide retained in DWMS released slowly, leading to the formation of lag phase.

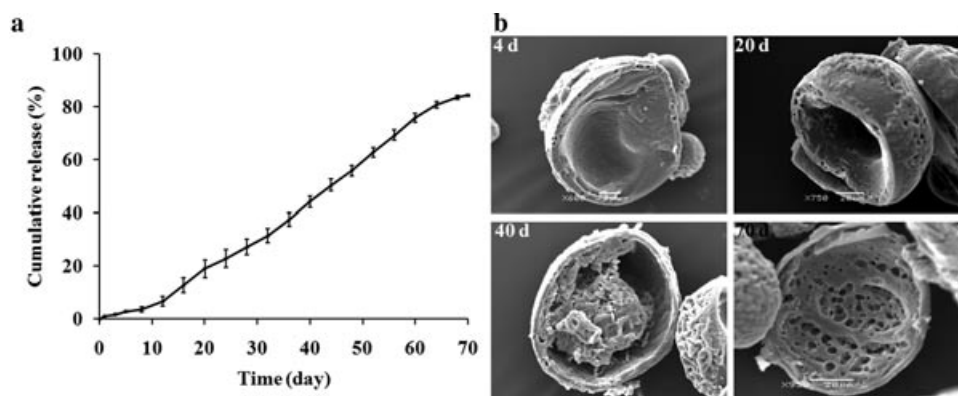


Figure 4. The *in vitro* release of exenatide from DWMS in PBS at 37°C. Data are means ± SE ($n = 3$). (a) SEM photographs of cross-sectional view of DWMS after different days of *in vitro* release. The pictures of upper left, upper right, lower left, lower right indicate the time of release experiment for 4, 20, 40, and 70 days, respectively (b).

After that, a near zero-order release up to 70 days was observed. About 84.4% of exenatide was released from DWMS at the end of 70 days, implying a completely release *in vivo*.

SEM photographs of cross-sectional view of DWMS taken from samples undergoing *in vitro* release experiments are shown in Figure 4b. After 4 days of undergoing *in vitro*, slightly degradation of PLGA core was observed. After 20, 40, and 70 days of release experiments, the inner core continued to degrade and disappear, and shrinkage in DWMS size was found. The PLLA coating was still relatively intact because its degradation rate is much lower than that of PLGA. The porous surface can be maintained at least 70 days, and the porous surface is a rate-controlling factor that makes the release of exenatide from the core near zero-order kinetics.

PK Model

The plots of observed and fitted exenatide concentration–time after s.c. administration at different doses are presented in Figures 5a–5c. After injection, due to burst release, exenatide concentrations increased rapidly, reaching initial peaks within 1 h, followed by a rapid decline through day 1. Owing to sustained release of DWMS, exenatide concentrations increased again after day 1 and reached their second peaks at about day 20. Twenty days later, the concentrations decreased slowly through day 50 at the end of determination. The proposed PK model nicely captured the overall profiles. VPC results showed that the proposed PK model could predict the exenatide concentrations closely and 12.5% of the observed concentrations fell outside the 90% prediction intervals (PIs) (Figs. 5a'–5c'). There was neither an initial period of high burst release nor an extended period with little or no release within the whole curve range after s.c. administration of exenatide DWMS to diabetic rats,

indicating that the release pattern of the constructed exenatide DWMS may have clinical significance due to the relatively stable exenatide concentration. The PK parameters were summarized in Table 1. All parameters were estimated with good precision (RSE% < 30% except for F_{ra2} at 31.1%). The results indicated that the time course of exenatide *in vivo* was in accord with linear PK under s.c. injection doses from 1.25–5 mg/rats.

PK/PD Model

Observed serum insulin concentration–time profiles after a single s.c. administration of vacant DWMS in diabetic rats were shown in Figure 6a. The solid dots and black line represent the individual values and mean value, respectively. The mean insulin level was constant in the experimental period, so the data were not considered in PK/PD model. The time courses of measured and fitted serum insulin concentrations after administration are shown in Figures 6b–6d. Serum insulin increased following DWMS treatment at three doses and remained elevated for 50 days. Insulin reached the first peaks at about 1 h, followed by a slow decrease through day 1. One day later, insulin concentrations increased slowly and got their secondary peaks at about day 10. This concentration–time profile of insulin is different from that of exenatide, in which the secondary peaks reached at about day 20. This may be explained by depletion of precursor pool of insulin. Ten days later, the serum insulin concentrations decreased slowly through day 50 at the end of determination. The proposed indirect response model was in good agreement with the insulin data. VPC indicated that the model manifested acceptable predictability and 7.8% of the observed insulin concentrations fell outside the 90% PI (Figs. 6b'–6d'). The estimated parameters with good precision (RSE% < 30%) are listed in Table 2. S_{m1} and

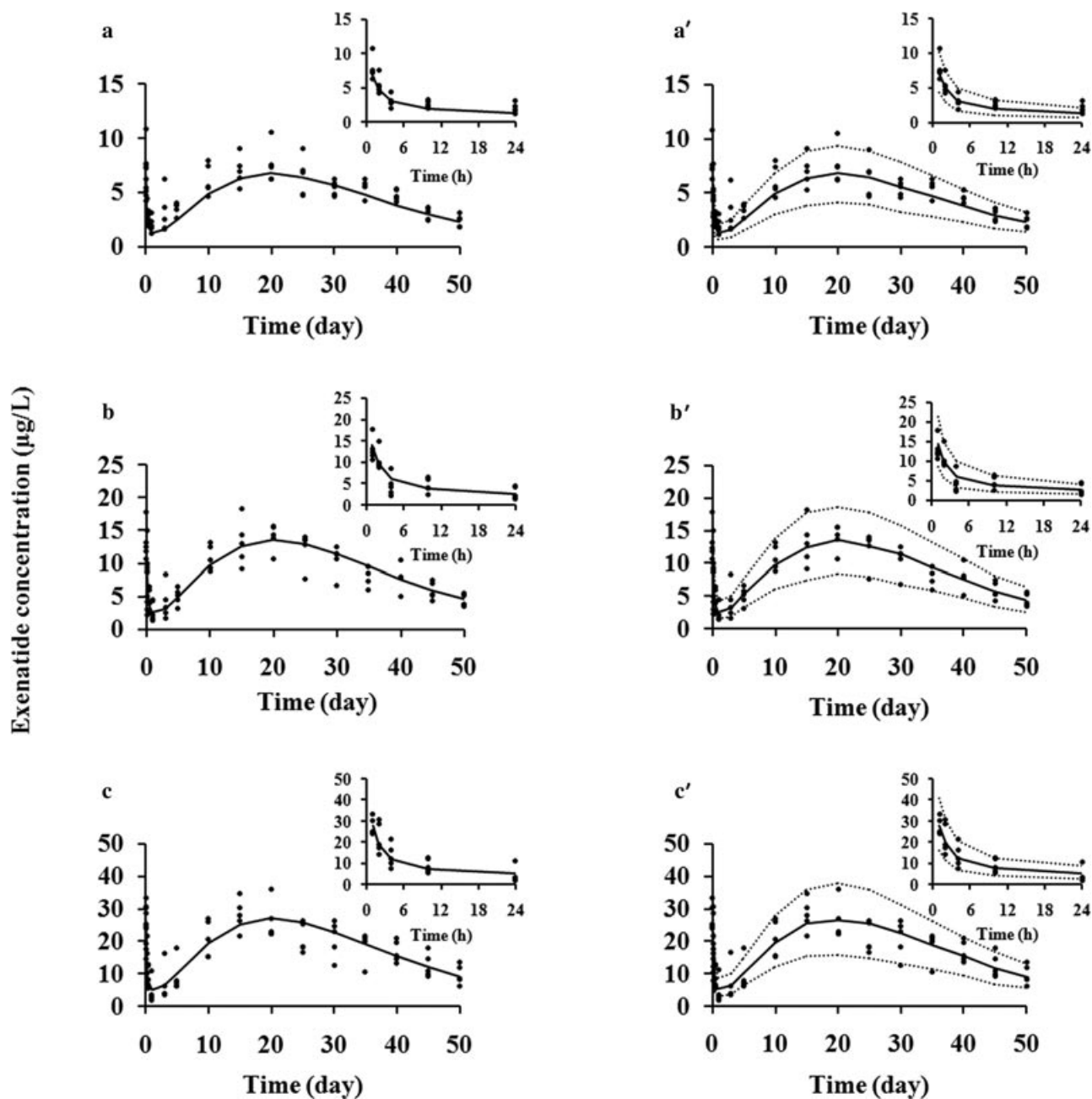


Figure 5. Observed and predicted serum exenatide concentration–time profiles after a single administration of DWMS at the exenatide dose of 1.25 (a), 2.5 (b), and 5 mg/rat (c) in diabetic rats. The solid dots represent individual data from rats and the solid line represents the model fit lines (a–c). Visual predictive check of serum exenatide concentration–time profiles after single administrations of DWMS at the exenatide dose of 1.25 (a'), 2.5 (b'), and 5 mg/rat (c'). The ranges between the dotted lines depict the 90% prediction intervals. The solid lines present the medians of simulated data. The solid dots are the observed concentrations. The inserts show the concentration versus time curves from 1 to 24 h (a'–c').

SC_{50} are drug-specific parameters, which are helpful for rational dosage regimen.

Figure 7 showed the observed blood glucose concentration–time profiles after a single s.c. DWMS at the exenatide dose of 0 (Fig. 7a), 1.25 (Fig. 7b), 2.5 (Fig. 7c), and 5 mg/rat (Fig. 7d) in diabetic rats. The solid dots and the black lines represent the individ-

ual data and mean values, respectively. The mean blood glucose level of control group increased from 29.5 to 31.4 mmol/L (Fig. 7a); therefore, it was necessary to transform the raw blood glucose to GLU. The observed and predicted GLUs after administration are displayed in Figures 8a–8c. Comparing with 1 h when insulin reached its first concentrations peaks,

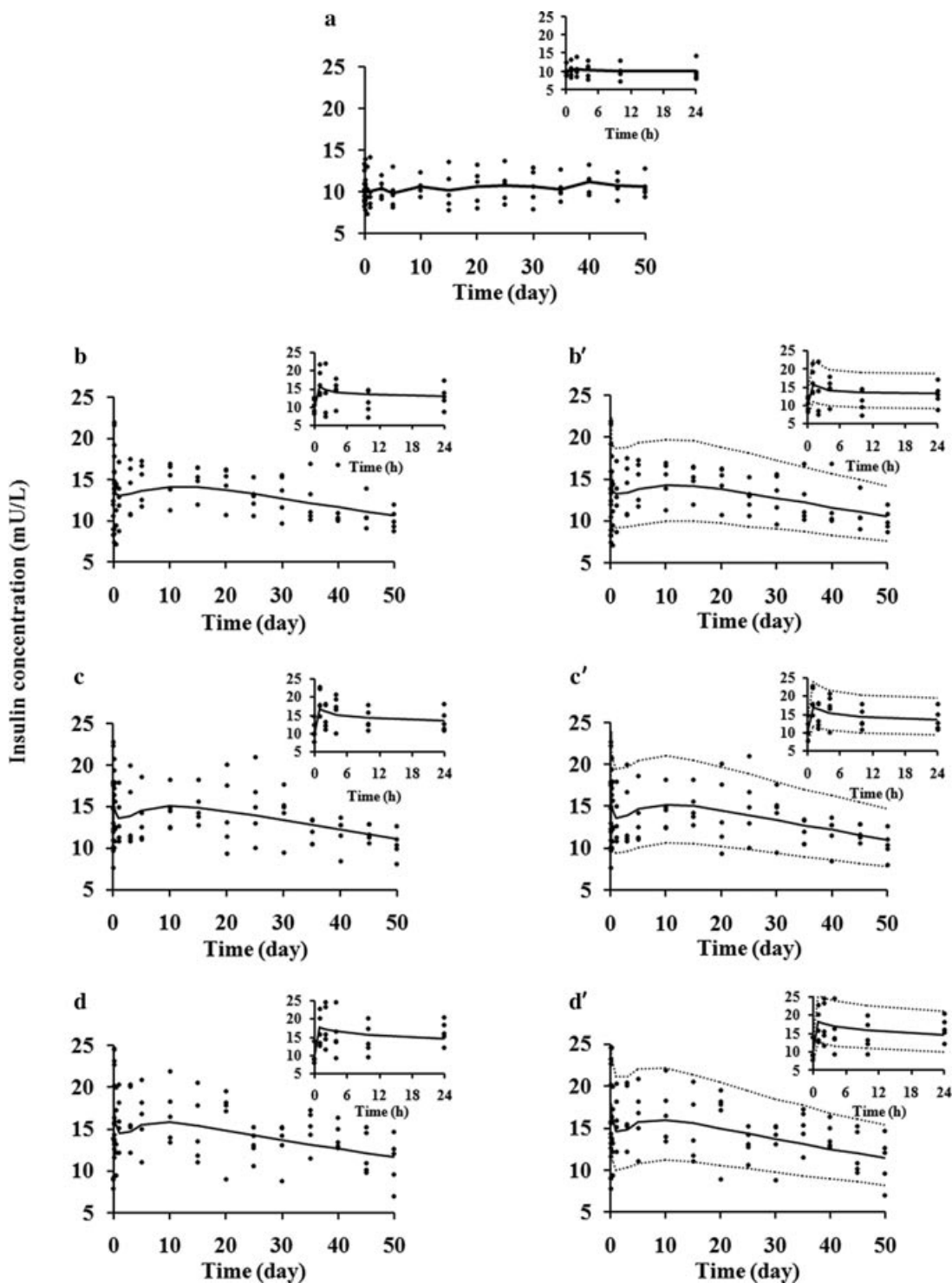


Figure 6. Observed serum insulin concentration–time profiles of control group, the solid dots and line represent the individual values and mean value, respectively. (a) Observed and predicted serum insulin concentration–time profiles after a single administration of DWMS at the exenatide dose of 1.25 (b), 2.5 (c), and 5 mg/rat (d) in diabetic rats. The solid dots represent individual data from rats and the solid line represents the model fit lines. (b–d). Visual predictive check of serum insulin concentration–time profiles after single administrations of DWMS at the exenatide dose of 1.25 (b'), 2.5 (c'), and 5 mg/rat (d'). The ranges between the dotted lines depict the 90% prediction intervals. The solid lines present the medians of simulated data. The solid dots are the observed insulin concentration. The inserts show the concentration versus time curves from 0 to 24 h (b'–d').

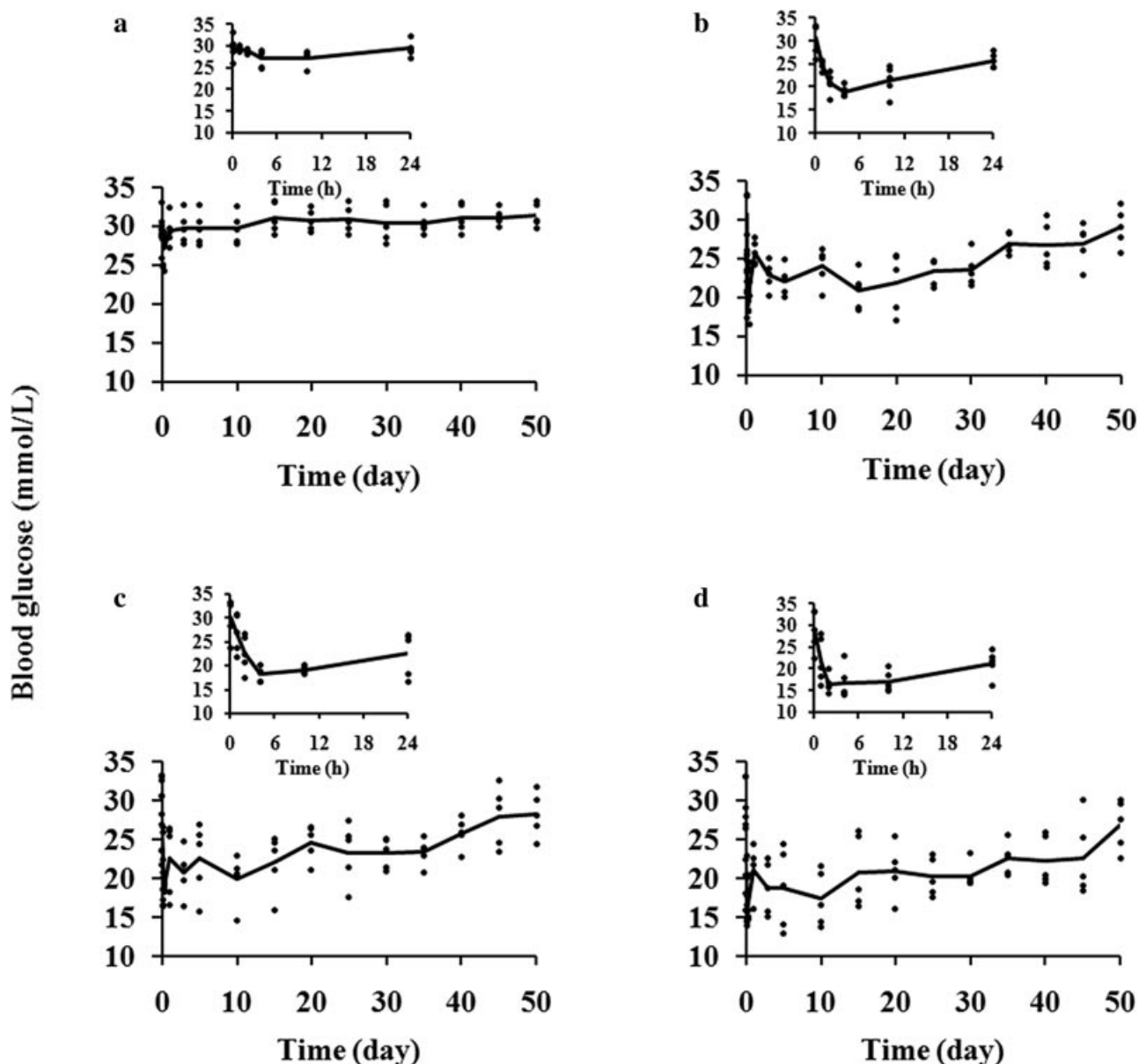


Figure 7. Observed blood glucose concentration–time profiles after a single s.c. administration of DWMS at the exenatide dose of 0 (a), 1.25 (b), 2.5 (c), and 5 mg/rat (d) in diabetic rats. The solid dots and black lines represent individual data and mean values from diabetic rats, respectively. The inserts show the blood glucose versus time curves from 0 to 24 h.

the time of maximal hypoglycemic effects are about 3–4 h after administration, showing significant time delay. Effect compartment and indirect response models nicely described this phenomenon. Owing to the reduction of insulin concentrations with time, the following GLUs increased slowly through day 1, followed by a decrease until day 10 and increase until the end of determination. VPC (Figs. 8a'–8c') showed that 8.2% of the observed GLUs fell outside the 90% PI, indicating that the final model has acceptable predictability.

In Vitro and *In Vivo* Correlation

The *in vivo* release profiles obtained from both deconvolution and simulation approaches were shown in Figure 3b. An initial burst release calculated from deconvolution and simulation were about 1.1% and 1.2%, respectively. The times to reach a plateau in *in vitro* release and *in vivo* experiment were 70 and 50 days, respectively. Therefore, the times required to reach plateau were normalized for the *in vitro* data.³¹ A scale factor of 1.4 (70 days divided by 50 days) was

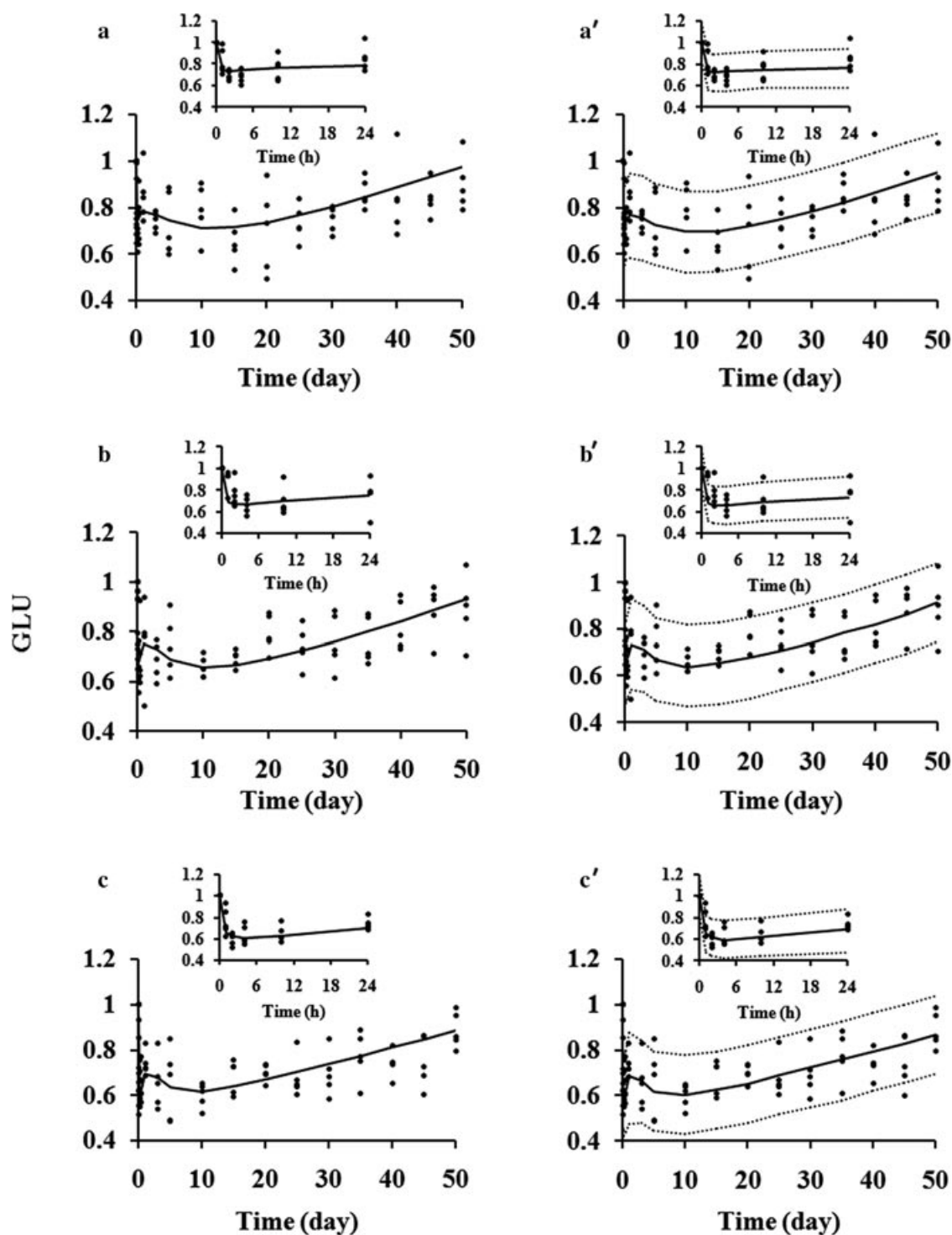


Figure 8. Observed and predicted GLU–time profiles after a single administration of DWMS at the exenatide dose of 1.25 (a), 2.5 (b), and 5 mg/rat (c) in diabetic rats. The solid dots and lines represent individual data from rats and the model fit lines, respectively. (a–c) Visual predictive check of GLU–time profiles after single administrations of DWMS at the exenatide dose of 1.25 (a'), 2.5 (b'), and 5 mg/rat (c'). The ranges between the dotted lines depict the 90% prediction intervals. The solid lines present the medians of simulated data. The solid dots are the observed GLU. The inserts show the GLU versus time curves from 0 to 24 h (a'–c').

employed here. All the *in vitro* times were divided by 1.4 and the time to reach plateau was the same with *in vivo* data. After normalization, the sampling times for the *in vitro* release and *in vivo* absorption data were not coincident, linear interpolation was used where necessary to obtain missing data.³⁶ This made it possible to establish a relationship between *in vitro* and *in vivo* release data, whereas time points were on the same scale. It has been recommended that burst release from systems such as microspheres should be investigated separately.³⁷ Therefore, the following lag phase and sustained release phase were used to establish a relationship between the *in vitro* and *in vivo* release data.

The linear regression plots of drug release (%) versus F_a for the exenatide DWMS are shown in Figure 3c and the relative regression equations are also inserted. The good linear regression correlation was demonstrated between the percentage of drug release in PBS at 37°C and the F_a (deconvolution: $R^2 = 0.982$, simulation: $R^2 = 0.984$). These results showed the drug absorption fraction *in vivo* could be predicted by the accumulated release percentage from *in vitro* test.

DISCUSSION

Because of low EE of DWMS prepared by water-in-oil-in-water evaporation method, we selected $O_1/O_2/W$ method to fabricate DWMS of exenatide.^{12,38,39} First, owing to the low solubility of exenatide in DCM, MeOH is added to the DCM as the mixed solvent to improve the solubility of exenatide.⁷ Second, because DWMS with particle size larger than 100 μm made from PLLA and PLGA^{12,38,39} necessitated the use of painfully large needles for the s.c. administration, low concentrations of PLGA and PLLA were used to prepare DWMS to reduce the particle size. Finally, the interfacial tensions and solvent evaporation rate are the critical factors for the formation of DWMS,¹⁰ and the high volatilization rate of solvent makes the phase separation not available, so we evaporate the solvent in the ice bath for 4 h to reduce the volatilization rate, and at room temperature for additional 4 h to evaporate the solvent completely.

PLLA and PLGA have different degradation rates, which achieved distinct degradation behavior and release patterns. The PLGA core underwent rapid and accelerated erosion, and the PLLA shell remained relatively intact even after 70 days *in vitro* due to its slow degradation. Rahman and Mathiowitz³⁹ investigated the influence of PLLA to PLGA ratio on the localization of bovine serum albumin (BSA) in DWMS. They found that using a PLLA–PLGA ratio of 1:1, FITC–BSA was localized in the PLLA shell, and with 1:2 and 1:3 PLLA to PLGA ratios, the FITC–BSA was localized in the PLGA inner core. In this study, the PLLA–PLGA ratio is 3:7 (between 1:2 and 1:3), and

most of exenatide was localized in the PLGA core of DWMS. The PLLA shell limits the release of exenatide in PLGA core, it is reasonable to anticipate that DWMS will provide a longer release time.¹³ Compared with exenatide PLGA microspheres,⁸ DWMS extend the *in vitro* and *in vivo* release period significantly. Porous surface (Figs. 2b and 2c) leads to the constant release of exenatide from DWMS after the lag phase of 8 days (Fig. 4a). Owing to a good IVIVC was observed for exenatide DWMS, the *in vivo* release behavior was similar with release *in vitro*. Constant *in vivo* release provided steady blood concentration of exenatide and GLUs. It was reported that the polymer ratio could significantly influence the release pattern¹³; therefore, to get an ideal release of DWMS, different PLLA–PLGA mass ratio was investigated in our preliminary experiments. The higher ratio of PLLA–PLGA were selected, the thicker shells were produced, the less burst release occurred, and the longer lag time and release period were observed. These results were consistent with their findings.¹³

Transit compartment model was widely used to describe both the oral drug absorption delays in pharmacokinetic analysis^{17–19} and the delayed effects for PD responses in signal transduction process.^{20–22} Here, it was employed to characterize the *in vivo* release of exenatide from DWMS for the first time. Microsphere compartment represents the PLGA core, and the first, second, and third transit compartments represent the three abstract compartments through which the exenatide release from PLGA core and PLLA shell to the surface of DWMS. The result of CLSM graph (Fig. 2d) showed that most of the exenatide located in the PLGA core, from which exenatide flow through the PLLA shell that was relatively intact in the whole release process (Fig. 4b). The release process of exenatide from PLGA core can be viewed as exenatide flowing through the sequential transit compartments. In addition, in PK model, the burst release was imitated by F_{ra4} , defined as fraction of exenatide in the absorption compartment with no lag release, directly coming from rapid release from the DWMS surface and/or near surface. Various numbers of transit compartments were investigated to link microsphere compartment to absorption compartment, and three transit compartments adequately characterized the lag phase and the following sustained-release phase. Such model-based method described the *in vivo* release of exenatide from DWMS nicely and quantitatively. To the best of our knowledge, this is the first time using transit compartment model to describe drug release from microspheres and to evaluate drug absorption *in vivo*.

As shown in Figures 8a–8c, expected GLUs diminished following continuous exenatide exposure. In fact, GLUs depended on the insulin concentration, and insulin secretion became weaker and weaker

as the time went on. This phenomenon could be explained by the depletion of a precursor pool, in which a certain amount of insulin was stored. Continuous exenatide exposure causes the liberation of insulin, and it may take a long time to replenish insulin in precursor pool. Precursor-dependent indirect response model was established successfully for characterizing this phenomenon. Moreover, considering the different sites of action for insulin, an effect compartment was integrated into our final PK/PD model. The stimulating effect of insulin on glucose elimination and inhibiting effects of insulin on glucose production were simulated by S_{m2} and I_m , respectively. Owing to sparse sampling for the exenatide DWMS, the parameters (k_{e0} , S_{m2} , k_{outG} , and I_m) were fixed as the previous estimated values (exenatide solution, dense sampling), which were more reliable. The small residual error indicated that the fixed values were reliable.

Because of the foreign body response,^{40,41} the *in vivo* degradation of polymer was faster than that *in vitro*, leading to the *in vitro* release of exenatide in PBS slower than that *in vivo*. The slower *in vitro* release has been reported in many PLGA-based release systems.^{31,42–44} It is difficult to use the *in vitro* conditions to simulate the *in vivo* conditions completely because of the complexity *in vivo*, such as the effect of tissue fluid on the polymer degradation, the presence of hydrolytic enzymes, and the pH gradient,⁴² but a simple release test is necessary as a quality control procedure to demonstrate performance and reproducibility in the preparation of DWMS.

Drug absorption after s.c. injection depends on the release of the drug from the microspheres, the dissolution of the drug under physiological conditions, and the permeability across the tissue barriers. In the case of exenatide DWMS, because exenatide has high dissolution and permeability, PLGA degradation and existence of PLLA shell are the rate-limiting factors for the *in vivo* behavior and a linear relationship between *in vivo* and *in vitro* can be expected. Deconvolution method is recommended by FDA to calculate the *in vivo* absorption profile from the plasma concentration–time curves, and a deconvolution-based level A IVIVC for exenatide DWMS was established in the present study. Furthermore, a simple model-based simulation method was proposed to calculate the *in vivo* absorption. The *in vivo* absorption curves obtained by deconvolution and that from simulation methods have a very good linear regression relationship ($R^2 = 0.999$). For model-based simulation method, the *in vivo* release profile was obtained from the simulated data, and goodness of fit is a key factor to evaluate the reliability of this method. The closer the fitted values to the observed values are, the more reliable the simulated results are. To our knowledge, this is the first time to use model-based simulation method to calculate the *in vivo* absorption and estab-

lish the level A IVIVC. The same approach may be used more widely for evaluation of the *in vivo* absorption and IVIVC of different drugs and formulations.

CONCLUSION

Exenatide DWMS with a near zero-order release profile after the lag phase was prepared using O₁/O₂/W method and was evaluated both *in vitro* and *in vivo*. Moreover, proposed PK/PD model described the hypoglycemic effect of exenatide DWMS in diabetic rats successfully. Transit compartment model was used to investigate the *in vivo* exenatide release from DWMS. IVIVCs were established by both deconvolution and model-based simulation methods. Our results showed that the proposed PK/PD model allowed a better understanding of the release profile and pharmacological properties of exenatide DWMS, and the model-based simulation may be useful in evaluation of *in vivo* release and IVIVC of sustained-release preparation.

ACKNOWLEDGMENTS

This work was supported by the Ministry of Science and Technology of the People's Republic of China (Peking University New Drug Research and Development Platform grant number 2009ZX09301-010).

REFERENCES

1. Parkes DG, Nielsen LL, Young AA. 2004. Pharmacology of exenatide (synthetic exendin-4): A potential therapeutic for improved glycemic control of type 2 diabetes. *Regul Pept* 117:77–88.
2. Young AA, Gedulin BR, Bhavsar S, Bodkin N, Jodka C, Hansen B, Denaro M. 1999. Glucose-lowering and insulin-sensitizing actions of exendin-4 - Studies in obese diabetic (ob/ob, db/db) mice, diabetic fatty Zucker rats, and diabetic rhesus monkeys (Macaca mulatta). *Diabetes* 48:1026–1034.
3. Kolterman OG, Kim DD, Shen L, Ruggles JA, Nielsen LL, Fineman MS, Baron AD. 2005. Pharmacokinetics, pharmacodynamics, and safety of exenatide in patients with type 2 diabetes mellitus. *Am J Health Syst Pharm* 62:173–181.
4. Parkes DG, Pittner R, Jodka C, Smith P, Young A. 2001. Insulinotropic actions of exendin-4 and glucagon-like peptide-1 *in vivo* and *in vitro*. *Metabolism* 50:583–589.
5. Krentz AJ, Patel MB, Bailey CJ. 2008. New drugs for type 2 diabetes mellitus: What is their place in therapy? *Drugs* 68:2131–2162.
6. Wright SG, Christenson T, Yeah TY, Rickey ME, Hotz JM, Kumar R, Costantino HR. 2008. Polymer-based sustained release device. Patent US7456254B2.
7. Kwak HH, Shim WS, Hwang S, Son MK, Kim YJ, Kim TH, Yoon ZH, Youn HJ, Lee GI, Kang SH, Shim CK. 2009. Pharmacokinetics and efficacy of a biweekly dosage formulation of exenatide in Zucker diabetic fatty (ZDF) rats. *Pharm Res* 26:2504–2512.
8. Yang HJ, Park IS, Na K. 2009. Biocompatible microspheres based on acetylated polysaccharide prepared from water-in-oil-in-water (W1/O/W2) double-emulsion method for delivery of type II diabetic drug (exenatide). *Colloids Surf A Physicochem Eng Aspects* 340:115–120.

9. Chen Y, Liu B, Dong QG, Wang MS, Shi L, Wu YG, Yu XH, Shi YY, Shan YM, Jiang CL, Zhang XZ, Gu TJ, Kong W. 2010. Preparation, characterization, and pharmacodynamics of exenatide-loaded poly(DL-lactic-co-glycolic acid) microspheres. *Chem Pharm Bull* 58:1474–1479.
10. Pekarek KJ, Jacob JS, Mathiowitz E. 1994. Double-walled polymer microspheres for controlled drug-release. *Nature* 367:258–260.
11. Zheng W. 2009. A water-in-oil-in-oil-in-water (W/O/O/W) method for producing drug-releasing, double-walled microspheres. *Int J Pharm* 374:90–95.
12. Tan EC, Lin R, Wang CH. 2005. Fabrication of double-walled microspheres for the sustained release of doxorubicin. *J Colloid Interface Sci* 291:135–143.
13. Berkland C, Cox A, Kim K, Pack DW. 2004. Three-month, zero-order piroxicam release from monodispersed double-walled microspheres of controlled shell thickness. *J Biomed Mater Res A* 70:576–584.
14. Pollauf EJ, Berkland C, Kim KK, Pack DW. 2005. *In vitro* degradation of polyanhydride/polyester core-shell double-wall microspheres. *Int J Pharm* 301:294–303.
15. Mathiowitz E, Leach KJP. 1998. Degradation of double-walled polymer microspheres of PLLA and P(CPP: SA)20: 80. I. *In vitro* degradation. *Biomaterials* 19:1973–1980.
16. Mathiowitz E, Leach KJP, Takahashi S. 1998. Degradation of double-walled polymer microspheres of PLLA and P(CPP: SA)20: 80. II. *in vivo* degradation. *Biomaterials* 19:1981–1988.
17. Savic RM, Jonker DM, Kerbusch T, Karlsson MO. 2007. Implementation of a transit compartment model for describing drug absorption in pharmacokinetic studies. *J Pharmacokinetic Pharmacodyn* 34:711–726.
18. Kagan L, Hoffman A. 2008. Selection of drug candidates for gastroretentive dosage forms: Pharmacokinetics following continuous intragastric mode of administration in a rat model. *Eur J Pharm Biopharm* 69:238–246.
19. Lehto P, Kortejarvi H, Liimatainen A, Ojala K, Kangas H, Hirvonen J, Tanninen VP, Peltonen L. 2011. Use of conventional surfactant media as surrogates for FaSSIF in simulating *in vivo* dissolution of BCS class II drugs. *Eur J Pharm Biopharm* 78:531–538.
20. Sun YN, Jusko WJ. 1998. Transit compartments versus gamma distribution function to model signal transduction processes in pharmacodynamics. *J Pharm Sci* 87:732–737.
21. Hamberg AK, Dahl ML, Barban M, Scordo MG, Wadelius M, Pengo V, Padrini R, Jonsson EN. 2007. A PK–PD model for predicting the impact of age, CYP2C9, and VKORC1 genotype on individualization of warfarin therapy. *Clin Pharmacol Ther* 81:529–538.
22. Li L, Li ZQ, Deng CH, Ning MR, Li HQ, Bi SS, Zhou TY, Lu W. 2012. A mechanism-based pharmacokinetic/pharmacodynamic model for CYP3A1/2 induction by dexamethasone in rats. *Acta Pharmacol Sin* 33:127–136.
23. Jiang W, Kim S, Zhang X, Lionberger RA, Davit BM, Conner DP, Yu LX. 2011. The role of predictive biopharmaceutical modeling and simulation in drug development and regulatory evaluation. *Int J Pharm* 418:151–160.
24. Landersdorfer CB, Jusko WJ. 2008. Pharmacokinetic/pharmacodynamic modelling in diabetes mellitus. *Clin Pharmacokinetic* 47:417–448.
25. Silber HE, Jauslin PM, Frey N, Karlsson MO. 2010. An integrated model for the glucose–insulin system. *Basic Clin Pharmacol Toxicol* 106:189–194.
26. Amidi M, Krudys KM, Snel CJ, Crommelin DJ, Della Pasqua OE, Hennink WE, Jiskoot W. 2008. Efficacy of pulmonary insulin delivery in diabetic rats: Use of a model-based approach in the evaluation of insulin powder formulations. *J Control Release* 127:257–266.
27. Ryan SM, Frias JM, Wang X, Sayers CT, Haddleton DM, Brayden DJ. 2011. PK/PD modelling of comb-shaped PEGylated salmon calcitonin conjugates of differing molecular weights. *J Control Release* 149:126–132.
28. Ackaert OW, De Graan J, Capancioni R, Della Pasqua OE, Dijkstra D, Westerink BH, Danhof M, Bouwstra JA. 2010. The *in vitro* and *in vivo* evaluation of new synthesized prodrugs of 5-OH-DPAT for iontophoretic delivery. *J Control Release* 144:296–305.
29. Sun Y, Wang J, Zhang X, Zhang Z, Zheng Y, Chen D, Zhang Q. 2008. Synchronic release of two hormonal contraceptives for about one month from the PLGA microspheres: *In vitro* and *in vivo* studies. *J Control Release* 129:192–199.
30. Jantravid E, De Maio V, Ronda E, Mattavelli V, Vertzoni M, Dressman JB. 2009. Application of biorelevant dissolution tests to the prediction of *in vivo* performance of diclofenac sodium from an oral modified-release pellet dosage form. *Eur J Pharm Sci* 37:434–441.
31. Zolnik BS, Burgess DJ. 2008. Evaluation of *in vivo*–*in vitro* release of dexamethasone from PLGA microspheres. *J Control Release* 127:137–145.
32. Buchwald P. 2003. Direct, differential-equation-based *in vitro*–*in vivo* correlation (IVIVC) method. *J Pharm Pharmacol* 55:495–504.
33. Sah H. 1997. A new strategy to determine the actual protein content of poly(lactide-co-glycolide) microspheres. *J Pharm Sci* 86:1315–1318.
34. Reed MJ, Meszaros K, Entes LJ, Claypool MD, Pinkett JG, Gadbois TM, Reaven GM. 2000. A new rat model of type 2 diabetes: The fat-fed, streptozotocin-treated rat. *Metabolism* 49:1390–1394.
35. Li XG, Li L, Zhou X, Chen Y, Ren YP, Zhou TY, Lu W. 2012. Pharmacokinetic/pharmacodynamic studies on exenatide in diabetic rats. *Acta Pharmacol Sin* (In press).
36. Balan G, Timmins P, Greene DS, Marathe PH. 2001. *In vitro*–*in vivo* correlation (IVIVC) models for metformin after administration of modified-release (MR) oral dosage forms to healthy human volunteers. *J Pharm Sci* 90:1176–1185.
37. Burgess DJ, Hussain AS, Ingallinera TS, Chen ML. 2002. Assuring quality and performance of sustained and controlled release parenterals: Workshop report. *AAPS PharmSci* 4:E7.
38. Kokai LE, Tan H, Jhunjhunwala S, Little SR, Frank JW, Marra KG. 2010. Protein bioactivity and polymer orientation is affected by stabilizer incorporation for double-walled microspheres. *J Control Release* 141:168–176.
39. Rahman NA, Mathiowitz E. 2004. Localization of bovine serum albumin in double-walled microspheres. *J Control Release* 94:163–175.
40. Spenlehauer G, Vert M, Benoit JP, Boddart A. 1989. *In vitro* and *in vivo* degradation of poly(D,L lactide/glycolide) type microspheres made by solvent evaporation method. *Biomaterials* 10:557–563.
41. Tracy MA, Ward KL, Firouzabadian L, Wang Y, Dong N, Qian R, Zhang Y. 1999. Factors affecting the degradation rate of poly(lactide-co-glycolide) microspheres *in vivo* and *in vitro*. *Biomaterials* 20:1057–1062.
42. Jiang G, Woo BH, Kang F, Singh J, DeLuca PP. 2002. Assessment of protein release kinetics, stability and protein polymer interaction of lysozyme encapsulated poly(D,L-lactide-co-glycolide) microspheres. *J Control Release* 79:137–145.
43. Jiang G, Qiu W, DeLuca PP. 2003. Preparation and *in vitro*/*in vivo* evaluation of insulin-loaded poly(acryloyl-hydroxyethyl starch)-PLGA composite microspheres. *Pharm Res* 20:452–459.
44. Machida Y, Onishi H, Kurita A, Hata H, Morikawa A. 2000. Pharmacokinetics of prolonged-release CPT-11-loaded microspheres in rats. *J Control Release* 66:159–175.